



Effect of Chelate Ring Size of Binuclear Copper(II) Complexes on Catecholase Activity and DNA Cleavage

Alana M. Homrich,^[a] Giliandro Farias,^[a] Suélen M. Amorim,^[a] Fernando R. Xavier,^[b] Rogério A. Gariani,^[b] Ademir Neves,^[a] Hernán Terenzi,^[c] and Rosely A. Peralta*^[a]

Catecholase activity of dicopper(II) complexes containing different numbers of chelate members in the pyridine groups of the ligand was studied to identify a functional model for copper enzyme catechol oxidase. Complexes $[\text{Cu}^{\text{II}}(\mu\text{-OH})\text{Cu}^{\text{II}}(\text{L}_1)](\text{ClO}_4)$ (1), $[\text{Cu}^{\text{II}}(\mu\text{-OH})\text{Cu}^{\text{II}}(\text{L}_2)](\text{ClO}_4)$ (2), and $[\text{Cu}^{\text{II}}(\mu\text{-OH})\text{Cu}^{\text{II}}(\text{L}_3)](\text{ClO}_4)$ (3) were synthesized and characterized by elemental analysis, FTIR, UV–Vis spectroscopy, mass spectrometry, and electrochemistry. Their catalytic activity in the oxidation of 3,5-di-*tert*-butylcatechol was determined. Changing the number of members of the

chelate rings altered the catalytic activity. Complex 2 showed the highest catalytic activity due to a high turnover rate, with efficiency of 3.40 ± 0.61 . Mechanistic investigations indicate that the catalytic reaction occurs through the reduction of Cu(II) to Cu(I) with formation of hydrogen peroxide. The spectroscopic and catecholase activity were further rationalized through DFT and TD-DFT calculations. Interestingly, all three complexes also showed DNA binding properties, which were also corroborated via molecular docking studies.

Introduction

Catechol oxidase (CO) is a copper-III enzyme that catalyzes the oxidation of *o*-diphenols into *o*-quinones.^[1] Through autopolymerization, *o*-quinones form melanin, a substance responsible for the darkening of plants or fruits. This process, known as enzymatic browning, plays a key role in protecting plants from pathogens and insect attack.^[2] Besides the *in vivo* activity, CO is also important for the determination of hormonal catecholamines (adrenaline, noradrenaline and dopamine),^[1a] which are related to a variety of neuronal malfunctions. The active center of catechol oxidase is composed of two copper(II) centers bridged by a μ -hydroxo, both coordinated by three histidine residues, which completes the coordination sphere of the copper(II) centers.^[1a,3]

Since the reporting of the CO structure, a large number of researchers have focused on the design and synthesis of complexes that can mimic the active site of the metalloenzyme and its function.^[4] The catecholase ability is dependent on many factors including the distance between the two metal centers, redox potential of the copper centers, pH and type of ligand.^[4a,5] In fact, over the last 30 years many mononuclear and dinuclear copper(II) complexes have been studied as biomimet-

ic models due to their ability to oxidize phenols and catechol. As a result, many model systems have been described and therefore various aspects of the catalytic mechanism.^[4a,6]

In the case of dicopper complexes, the catecholase activity is dependent on the design of the ligands, since the two metal ions are fixed in close proximity and this strongly affects the properties and reactivity of the complexes. In this regard, the nature of the atom donors, the flexibility of the ligand and, thus, the geometric features of the complex are of great interest in the synthesis of small molecules that can mimic the active sites of different metalloenzymes and are currently a focus in research studies. However, the majority of ligands reported have a five-membered chelate ring and the influence of the number of members of the chelate ring around the copper(II) atoms has not been evaluated.^[7]

Copper is also a bio-essential element and copper complexes can play several biological roles *in vivo*, such as: antibacterial,^[8] antifungal, antimicrobial, and anticancer/antiproliferative activity.^[9] Indeed, the study of the interaction of copper complexes with DNA is an important field of research since these complexes can cleave DNA under physiological conditions.^[10] This ability merits attention considering that it can produce fragments similar to those formed by restriction enzymes.^[5a,11]

In this paper, we report the synthesis, characterization, catecholase activity and DNase activity of three new dicopper (II) complexes. These complexes differ by way of a modification in the spacers between the pyridine and the tertiary amine of the ligands, giving them different degrees of flexibility. The ligands H_2L_1 and H_2L_2 have been previously reported in the literature^[12] and ligand H_2L_3 is new (Figure 1). Modifications to the initial ligand H_2L_1 (Figure 1a) were carried out to probe the effect of the number of chelate ring members, when methyl spacers are changed to ethyl spacers (Figure 1b and Figure 1c), on the enzyme mimicking (catecholase and DNase). This effect was evaluated through spectroscopic and theoretical methods.

[a] A. M. Homrich, G. Farias, Dr. S. M. Amorim, Prof. A. Neves, Prof. R. A. Peralta
Federal University of Santa Catarina
88040900, Florianópolis, SC, Brazil
E-mail: rosely.peralta@ufsc.br

[b] Prof. F. R. Xavier, Prof. R. A. Gariani
Department of Chemistry
State University of Santa Catarina
89219-710, Joinville, SC, Brazil

[c] Prof. H. Terenzi
Department of Biochemistry
Federal University of Santa Catarina
88040900, Florianópolis, SC, Brazil

Supporting information for this article is available on the WWW under
<https://doi.org/10.1002/ejic.202001170>

Part of the "Inorganic Chemistry in Latin America" Special Collection.

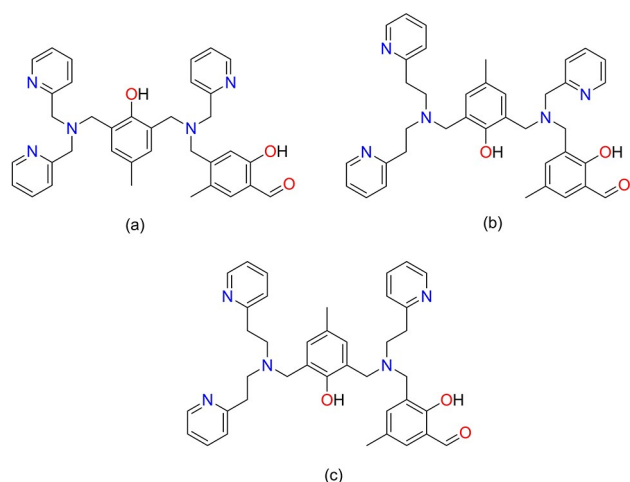


Figure 1. Ligands used in this study: (a) H_2L_1 , (b) H_2L_2 and (c) H_2L_3 .

Results and Discussion

Design and characterization of the copper(II) complexes

The ligands H_2L_1 , H_2L_2 and H_2L_3 (Figures S1, S2 and S3, respectively) were obtained for the synthesis of the complexes (Figure S4) and their characterization can be found in the Supporting Information (Figure S5–S10). Due to structural differences between the ligands (Figure 2), complex **1** is formed of only five-membered chelate rings, while complex **2** is formed of six-membered chelate rings in the soft portion of the ligand

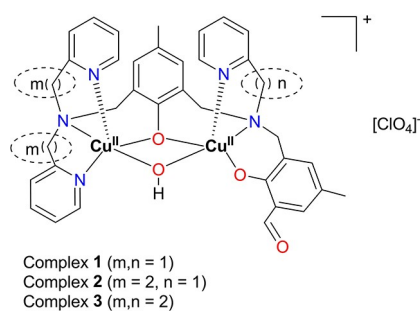


Figure 2. Structural representation of complexes 1–3.

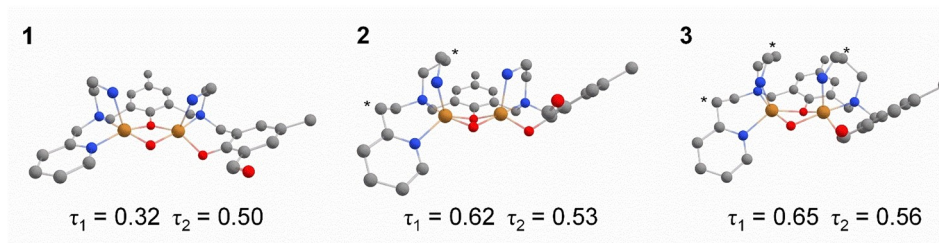


Figure 3. Optimized ground state geometries for complexes **1**, **2** and **3** using BP86/Def2-TZVP (metals) or Def2-SVP (all others). Some atoms are omitted and the carbons that have been added are marked with an asterisk for clarity.

and five-membered rings in the hard portion. Complex **3** is formed by six-membered chelate rings surrounding the pyridines and by a five-membered chelate ring with the phenolic substituted aldehyde (Figure 2).

The coordination of the ligand was initially observed by infrared spectroscopy (Figure S11–13 and Table S1). The major bands assigned to the ligands are also present in the spectra for the complexes with some energetic shifts due to complexation. The spectra of the complexes also feature new bands, such as an intense band at 1070 cm^{-1} attributed to the perchlorate counterion.^[13] The results obtained for complexes **1–3** are in agreement with those reported in the literature for systems with similar N,O-donor ligands.^[5a,11c]

In order to obtain further information, density functional theory (DFT) was used to predict likely structures for complexes **1–3** and their conjugates with the 3,5-DTBC. The optimization of the structures for the three complexes was carried out with an μ -OH bridge between the copper atoms due to the fast exchange of the acetate bridge in solution and without any water molecule coordinated to the copper atoms, as reported by Peralta and co-workers^[11c] for a similar Cu^{II} complex. The possibility that the unpaired electron associated with Cu_1 and Cu_2 may interact, ferromagnetically ($S=1$) or antiferromagnetically ($S=0$), was evaluated. For all complexes, the high spin surface is in the ground state and the low spin surface is at 9.3 kJ mol^{-1} for **1**, 1.3 kJ mol^{-1} for **2** and 3.6 kJ mol^{-1} for **3**. The hybrid functional PBE0 was also used to confirm the high spin ground state. These theoretical results confirm that one unpaired electron is associated with the Cu atoms, which is in agreement with previous experimental measurements^[11c] and theoretical studies^[14] for similar compounds. Therefore, the open-shell triplet state was considered in the calculations. Also, for complexes **2** and **3** the conformer possibilities due to the differences between ligands were evaluated and are described in the Supporting Information (Figure S14–15).

The optimized geometries of the three complexes are shown in Figure 3. For each Cu^{II} the structural index parameter was calculated for all complexes, showing that for **1** the environment around the Cu_1 center (τ_1) is closer to a distorted square pyramidal geometry while the Cu_2 atom (τ_2) shows an intermediate geometry between distorted square pyramidal and distorted trigonal-bipyramidal geometry, as reflected by the structural index parameter of $\tau_2=0.5$. On other hand, for complexes **2** and **3**, the environment around both Cu atoms is

closer to a distorted trigonal-bipyramidal geometry for these complexes. As can be seen in Table S2, all of the bonds around the copper atom were in good agreement with those previously reported for binuclear Cu^{II} complexes for which X-ray structures have been obtained.^[11c] The calculated vibrational frequencies and intensities were compared with the experimental infrared spectra (Figure S16–S18) and showed reasonable agreement with the experimental data. Table S3 shows the assignments of the IR bands for complexes 1–3 based on these calculations.

Therefore, for these complexes, **1** formed of only five-membered chelate rings, while in complexes **2** and **3** these rings are increased to form six-membered chelate rings, resulted in a distortion of the geometry environment around both Cu atoms. An intermediate geometry between distorted square pyramidal and distorted trigonal-bipyramidal geometry was obtained for **1** and a majority distorted trigonal-bipyramidal geometry for **2** and **3**.

Solution studies

The mass spectra for complexes **1** (Figure S19), **2** (Figure S20) and **3** (Figure S21) show peaks at $m/z = 742.15$, 756.26 and 786.20 , respectively. For complexes **1** and **3**, the isotopic distribution is consistent with a $[\text{Cu}^{\text{II}}(\mu\text{-OCH}_3)\text{Cu}^{\text{II}}(\text{L})]^{2+}$ fragment, indicating that, under the conditions of ESI-MS in methanolic solution, there was the exchange of the $\mu\text{-OH}$ bridge for $\mu\text{-OCH}_3$. For complex **2**, the isotopic distribution is consistent with a $[\text{Cu}^{\text{II}}(\mu\text{-OH})\text{Cu}^{\text{II}}(\text{L}_2)]^{2+}$ fragment. In the electronic spectra of complexes **1**, **2** and **3** (Figure S22–24) there is an intense band between 340–390 nm, which is attributed to the sum of intraligand transitions and charge transfer from phenolate to copper ion (ligand to metal charge transfer - LMCT). The band at 450 nm refers to the phenolate-Cu^{II} LMCT and a less intense band, at approximately 650 nm, is due to the $d\text{-}d$ transitions of the copper atoms.^[15] The electronic profile revealed for the three cases is similar to those observed in some related systems.^[5a,11c,16] Differences in the phenolate orientation toward Cu^{II} may be associated with the change in the probability of LMCT occurring in the complex.^[17]

Time-dependent DFT (TD-DFT) was used to simulate the absorption spectra and thus better understand the assignment of the data in the experimental spectra. Based on these calculations, the low energy bands at approximately 650 nm in the experimental spectra for complexes 1–3 can be resolved in a few excitations, all of which are related to $d\text{-}d$ -like transitions, with donor and acceptor molecular orbitals making a small contribution to the coordinated oxygen atoms or from the pyridine moieties to the donor. The hypsochromic shift observed in these $d\text{-}d$ -like transitions seems to be related to the net results of the most intense transitions, which are low energy $d\text{-}d$ -like transitions for complex **1**, intermediate energy $d\text{-}d$ -like transitions for **2**, and high energy transitions for **3** (Table S4). Also, the higher oscillator strength observed for these $d\text{-}d$ -like transitions for complexes **2** and **3** follows the same trend as the molar absorptivity. The shoulder observed in the experimental absorption spectra around 450–500 nm is ascribed to a LMCT

from the phenolate moieties to the Cu^{II}. The remaining transitions at the high energy end of the spectrum are $\pi\text{-}\pi^*$ like transitions. Theoretical absorption spectra along with the excitations with a major contribution to each excited state are shown in Figure 4 for complex **1**. Further information on the states with the most intense calculated transition for each convoluted band is given in Table S4.

The redox behavior of the complexes was investigated via square wave voltammetry (Figure S25). The voltammograms presented two processes, assigned to the pairs Cu^{II}Cu^{II}/Cu^ICu^I and Cu^{II}Cu^I/Cu^ICu^I. According to Table 1 and Figure S25, the metal centers of complex **3** are more easily reduced. Increasing the chelate ring size promoted an anodic shift in the half-wave potential of the complexes, as previously observed.^[16c] Higher stabilization of the Cu^I species in the less rigid complex is expected, as the reduction of Cu^{II} changes the preferred geometry of the metal system.^[18] Also, as seen in Table S2, the average bond lengths around the basal plane of the Cu₁ and Cu₂ atoms are 2.032 Å for **1**, 2.049 Å for **2** and 2.055 Å for **3**. This larger bond length should reduce the electronic density over the metal and facilitate the reduction process.

The chemical equilibrium between the species of the complexes present in solution were determined by spectrophotometric titration. Table 2 shows the deprotonation constants of the complexes and the proposed assignment of the corresponding equilibrium processes is shown in Figure S26.

The pK_{a1} values correspond to the lateral phenol deprotonation. During titration, an increase in the pH coinciding with an increase in the band at 400 nm, according to the electron spectroscopy studies (Figure S27–29), suggests a higher probability of LMCT occurrence. The values determined and the attributions are in agreement with results reported by Peralta et al.^[5a] for similar complexes. The second pK_a is attributed to the formation of the hydroxo bridge between the metals, in agreement with the pK_{a2} value obtained for the $[\text{Cu}^{\text{II}}(\mu\text{-OH})\text{Cu}^{\text{II}}(\text{HBTPPNOL})]^{2+}$ complex.^[19] The pK_{a3} refers to the coordinated deprotonation of water to one of the Cu^{II} centers,

Table 1. Electronic spectral and electrochemical data for complexes 1–3.

	λ_{max} [nm] (ϵ [mol ⁻¹ L cm ⁻¹])		$E_{1/2}$ [mV vs NHE] ^[a]
	CH ₃ OH	CH ₂ Cl ₂	
1	700 (166); 358 (3802)	845 (149); 660 (shoulder); 341 (1560)	−0.72 −0.42
2	656 (265); 460 (shoulder); 379 (8890)	672 (182); 378 (3717)	−0.66 −0.45
3	600 (247); 450 (shoulder); 387 (2202)	622 (154); 340 (1718)	−0.59 −0.35

[a] Measured in MeOH solution at concentration of 1×10^{-3} mol L⁻¹.

Table 2. Spectrophotometric pK_a values for complexes 1–3.

	pK _{a1}	pK _{a2}	pK _{a3}
1	4.73 ± 0.01	6.66 ± 0.1	7.86 ± 0.2
2	4.41 ± 0.02	6.42 ± 0.1	7.54 ± 0.1
3	4.23 ± 0.04	5.80 ± 0.03	7.41 ± 0.1

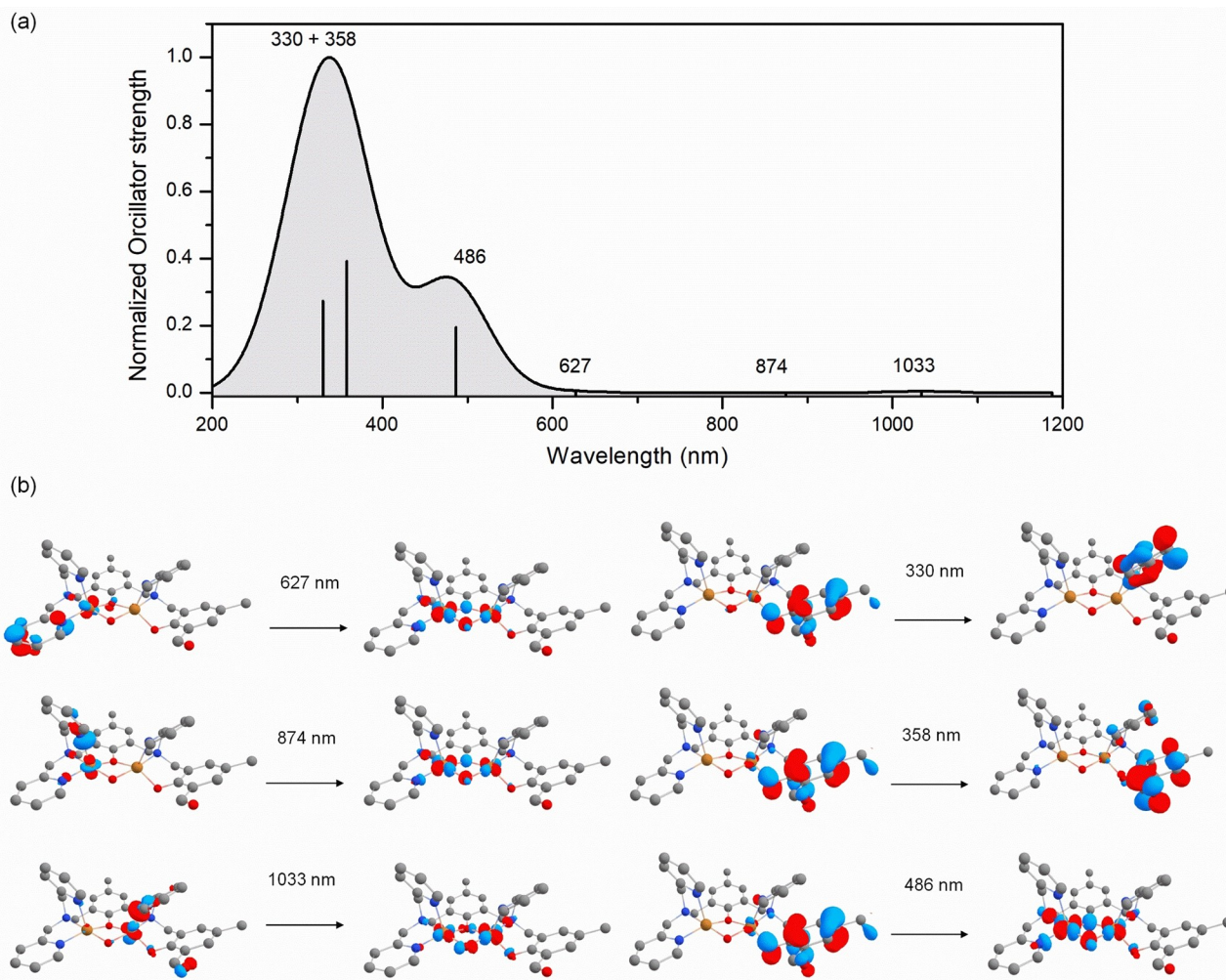


Figure 4. (a) Theoretical absorption spectra for complex 1 convoluted with Gaussians of 100 nm width along with the most intense calculated transitions for each convoluted band and (b) excitations with a major contribution to each excited state showed in the theoretical absorption.

approaching results observed for similar systems.^[5a,11c] In addition to the redox potential values obtained for the systems, an increase in the chelate ring size also affects the pKa values for the species, making **3** the most acidic complex in the series. The distribution of the species of complexes **1**, **2** and **3** as a function of pH is shown in Figures S30–S32.

Catecholase activity

Different kinetics assays to study the oxidation of the 3,5-di-*tert*-butylcatechol (3,5-DTBC) substrate were performed with the complexes. For each experiment, the initial reaction rate was obtained from the slope of the absorbance plotted as a function of time in the first minutes of the reaction. Initially, by shifting the pH of the reaction medium (Figure 5), it was observed that the catalytically active species is $[\text{Cu}^{\text{II}}(\mu\text{-OH})\text{Cu}^{\text{II}}(\text{OH})(\text{L})]$, which is predominant at pH 9.0 (Figures S30–S32).

Significant changes in the initial reaction rate occur only after pH 7.0 and thus the catalytic activity of other species can

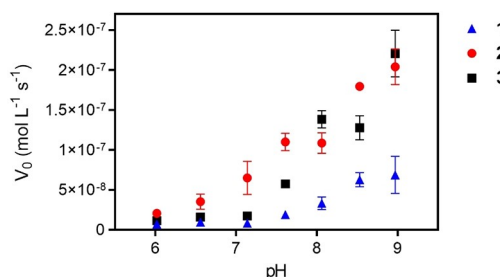


Figure 5. Dependence of the initial reaction rate (V_0) on the pH value in 3,5-DTBC oxidation catalyzed by complexes **1**, **2** and **3**. Conditions: $[\text{1}] = 18 \mu\text{mol L}^{-1}$, $[\text{2}] = [\text{3}] = 25 \mu\text{mol L}^{-1}$, $[\text{3,5-DTBC}] = 5 \text{mmol L}^{-1}$, $[\text{buffer}] = 30.3 \text{mmol L}^{-1}$ (pH 6.0–9.0), solution of $\text{CH}_3\text{OH}/\text{H}_2\text{O}$ (32:1, v/v), $T = 25^\circ\text{C}$.

be considered to be low. Several researchers have suggested that the presence of a terminal hydroxo group coordinated to the copper center aids the substrate deprotonation, facilitating its coordination.^[5f,20]

The effect of substrate concentration was evaluated at pH 9.0 and all complexes reached a saturation profile (Figure 6).

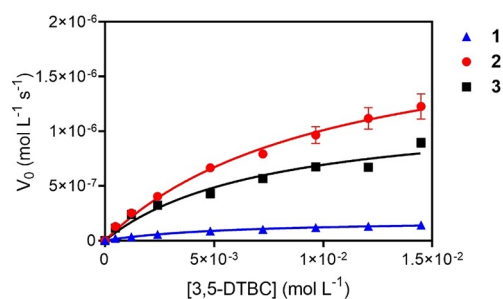


Figure 6. Dependence of the initial reaction rate (V_0) on the 3,5-DTBC concentration for the oxidation reaction catalyzed by complexes 1, 2 and 3. Conditions: [Complex] = $60 \mu\text{mol L}^{-1}$, [3,5-DTBC] = 4.90×10^{-4} – $1.45 \times 10^{-2} \text{ mol L}^{-1}$; [buffer] = TRIS (30.3 mmol L^{-1} , pH 9.0) solution of $\text{CH}_3\text{OH}/\text{H}_2\text{O}$ (32:1, v/v), $T = 25^\circ\text{C}$.

The Michaelis-Menten model^[21] was applied and the kinetic parameters were obtained (Table 3).

The turnover rates (k_{cat}) for complex 2 and 3 were, respectively, around 11 and 6 times higher than that of complex 1. Although it had the largest K_{ass} value, complex 1 was the least efficient of the series, indicating that an increase in the size of the chelate rings enhances the flexibility of the ligand and promotes the catalysis of this reaction. The change from five to six members in the chelate ring, in the hard portion of the ligand, in complex 3 facilitates the complex-substrate association, but the k_{cat} value for complex 2 is higher, contributing to it having the highest catalytic efficiency of the series. It is clear that the catalytic constants obtained for complexes 2 and 3 are notable when compared to other biomimetic complexes that have similar N,O-donor ligands (Table 3).

To improve the discussion, the 3,5-DTBC conjugates for complexes 1–3 were also optimized, as described in the Supporting Information (Figure S33–S35). For these complexes, we found two possibilities which are in agreement with previous reports,^[22] one removing the hydroxo bridge and with 3,5-DTBC in a $\eta^2:\eta^1$ binding mode and one with the bridge and with a *syn-syn* binding mode. In both cases, as described for other similar complexes, the larger k_{cat} values for catecholase activity of complex 2 and 3 compared to 1, can be attributed to the lower Cu–Cu distance for conjugate complexes of 1, 2 and

3 of 3.067, 2.979 and 3.059 Å, respectively, for the complexes with the bridge. These values are 3.087, 3.038 and 3.067 Å, respectively, for complexes with the $\eta^2:\eta^1$ binding mode. Also, the higher flexibility of the ligand with 6-membered ring in complexes 2 and 3, can accommodate better the substrate.

Furthermore, in the two cases, the 3,5-DTBC interacts in different ways with the complex, which should reflect in the K_{ass} values observed experimentally. For the complexes with the hydroxo bridge, the variation in the K_{ass} values was attributed to the orientation of the 3,5-DTBC. In the case of complex 1, with the highest K_{ass} value, the most stable optimized 3,5-DTBC conjugate showed a π -stack interaction between the ligand and the substrate, while for 2 and 3 the most stable optimized 3,5-DTBC conjugate did not show this interaction. In the conjugates with a $\eta^2:\eta^1$ binding mode, for complex 1 there was a similar π -stack interaction while for 2 and 3 interaction with the closer pyridine moiety was observed. Therefore, both possibilities of conjugate complexes may exist in solution, but the verification of these species requires further analysis, which is out of the scope of this work.

During the reaction catalyzed by complexes 1–3, there is hydrogen peroxide generation, evidenced by the iodometry method.^[5f,23] Thus, although they are biomimetics of catechol oxidase, the catalysis mechanism differs from that associated with the enzyme, which produces only water. In the presence of the complexes, therefore, the reaction stoichiometry is $3,5\text{-DTBC} + \text{O}_2 \rightarrow 3,5\text{-DTBQ} + \text{H}_2\text{O}_2$. According to inert atmosphere tests, molecular oxygen is directly involved in the catalytic cycle, probably re-oxidizing Cu^{I} centers after the formation of a quinone equivalent. Considering the previously discussed data and the theoretical modelling, a probable mechanism is shown in Scheme 1 for complex 1, which is in agreement with the mechanism described by Neves and co-workers for a similar complex.^[20b] The mechanism for complexes 2 and 3 differs only in terms of the orientation of 3,5-DTBC.

DNA cleavage activity

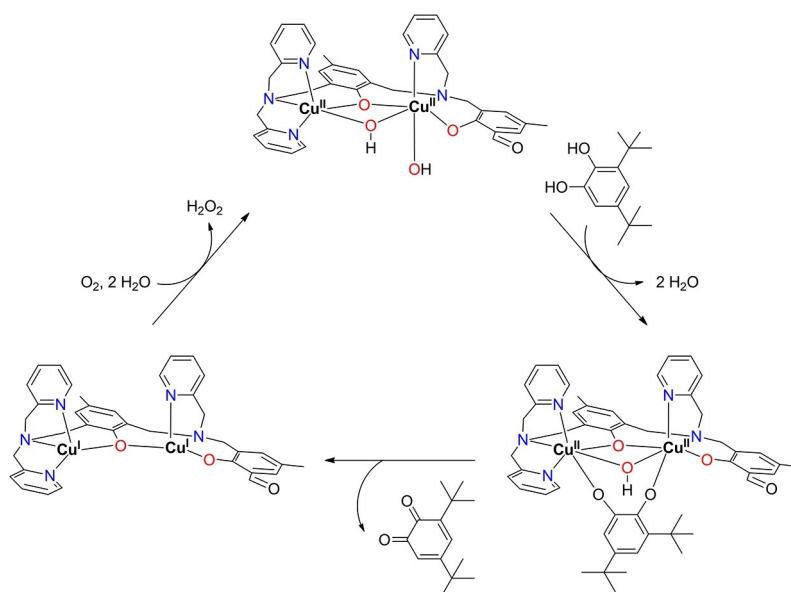
Initially, the cleavage of plasmid DNA promoted by complexes 1–3 was performed at different pH values (Figure S36). These assays indicate that all complexes are capable of cleaving plasmid DNA and the highest activity was observed at pH 6.0. The effect of the complex concentration on DNA cleavage was then investigated (Figure 7).

There was a significant difference in the levels of activity observed for the complexes studied. Complex 3 cleaved around 50% of the DNA at a concentration of only $0.5 \mu\text{mol L}^{-1}$ while this level of cleavage was achieved by the other complexes (1 and 2) only at a concentration of $5 \mu\text{mol L}^{-1}$.

To understand the forms of interaction between the complexes and DNA, studies have been conducted increasing the ionic strength of the reaction medium. We observed that DNA cleavage by the complexes gradually decreases as the sodium chloride concentration in the reaction increases (Figure S37). Assays were also performed in the presence of lithium perchlorate (Figure S38) and again there was inhibition of

	k_{cat} [10^{-3} s^{-1}]	K_{M} [$10^{-3} \text{ mol L}^{-1}$]	$K_{\text{ass}}^{\text{[a]}}$ [L mol^{-1}]	$E^{\text{[b]}}$ [$\text{L mol}^{-1} \text{ s}^{-1}$]
1	3.17 ± 0.23	5.77 ± 0.60	173.31 ± 0.10	0.60 ± 0.08
2	34.08 ± 3.50	10.26 ± 1.50	97.47 ± 0.15	3.40 ± 0.61
3	20.12 ± 2.97	7.42 ± 1.44	134.77 ± 0.19	2.86 ± 0.70
Ref. [4e]	29.61	4.90	204	6.04
Ref. [4f]	0.78	1.66	602	0.45
Ref. [5a]	5.83	8.93	112	0.65
Ref. [11c]	5.33	3.96	252	1.35
Ref. [19]	2.80	0.86	1162	3.3

[a] $K_{\text{ass}} = 1/K_{\text{M}}$. [b] $E = k_{\text{cat}}/K_{\text{M}}$.



Scheme 1. Proposed mechanism for the oxidation of 3,5-DTBC catalyzed by complex 1.

plasmid DNA cleavage by the complexes. The same results were obtained in the presence of both salts (NaCl/LiClO₄), indicating that the inhibition is due to interaction between the cationic part of the salts and the anionic DNA skeleton rather than interaction between the salts and the complexes. Similar results have been reported in the literature.^[59,24]

Assays in the presence of groove ligands indicate that, in addition to being electrostatically attracted to DNA, the complexes interact with B-DNA through their major and minor grooves (Figure S39). The three complexes have no preference for any of the grooves, and their activity was reduced in the presence of netropsin or methyl green. DNA circular dichroism spectra obtained with different concentrations of complexes 1, 2 and 3 show that the complexes can modify the helical structure of DNA by altering the nitrogen base pairing.^[25] Figure 8 shows that there is a reduction in the intensity of the bands characteristic of B-DNA (275 and 245 nm), which is distinct from the behavior of intercalating molecules.^[26] Thus, complexes 1, 2 and 3 probably interact with DNA through electrostatic attraction with the anionic skeleton and binding to the larger and smaller grooves of B-DNA.

Regarding the cleavage mechanism, studies were performed in the presence of different reactive oxygen species sequestrants. The results suggest that the mechanism involves an oxidative pathway, with the generation of hydrogen peroxide and singlet oxygen species (Figure S40). Several copper(II) complexes cleave DNA oxidatively, mainly with the addition of co-reagents.^[27] In this case, complexes 1, 2 and 3 can oxidatively cleave plasmid DNA even in the absence of co-reagents. Tests carried out in an argon atmosphere also corroborate the oxidative mechanism, with a decrease in the activity of the complexes in the absence of molecular oxygen (Figure S41).

In the presence of sodium ascorbate as a co-reagent, the activity of complexes 1, 2 and 3 can be modulated (Figure 9).

The addition of the reducing agent leads to an increase in the reduction of Cu^{II} to Cu^I centers and the generation of hydroxyl radicals through Fenton-type reactions.

Complexes 1, 2 and 3 are able to cleave plasmid DNA in the absence of co-reagents, as observed in previous assays, upon incubation periods of 4 h at 50 °C. With the addition of sodium ascorbate, the reaction time was substantially reduced, even at a lower reaction temperature, indeed there was approximately a 2 to 9-fold increase in the plasmid DNA cleavage (Table S5). For the efficient use of complexes as drugs in cells with more or less reducing environments, it is of great interest that their activity can be modulated by the addition of co-reagents.

Finally, studies on the kinetics of plasmid DNA cleavage by complexes were performed by changing the catalyst concentration (Figure 10). The kinetics parameters were obtained through the Michaelis-Menten equation^[21] and the results can be seen in Table 4.

The catalytic efficiency of complex 3 ($k_{\text{cat}}/K_{\text{M}}$) is higher compared with 1 and 2 (Table 4), in agreement with the tendency evidenced with regard to the effect of complex concentration on DNA ($3 > 2 > 1$). Thus, in the DNA cleavage,

Table 4. Kinetics parameters for the plasmid DNA cleavage catalyzed by the complexes.

	k_{cat} [h ⁻¹]	K_{M} [10 ⁻⁶ mol L ⁻¹]	$k_{\text{cat}}/K_{\text{M}}$ [10 ³ L mol ⁻¹ h ⁻¹]	$k_{\text{cat}}/k_{\text{unc}}^{[a]}$ [10 ⁶]	$t_{1/2}$ [h]
1	0.19 ± 0.07	23.72 ± 8.75	8.16	1.29	3.58
2	0.20 ± 0.05	14.84 ± 6.81	13.57	1.34	3.44
3	0.27 ± 0.06	8.71 ± 3.50	31.46	1.83	2.53
Ref. [5f]	0.12	120.0	1.0	0.8	5.8
Ref. [28]	0.061	18.0	3.39	0.41	11.34

[a] $k_{\text{unc}} = 1.5 \times 10^{-7} \text{ h}^{-1}$, ref.^[29]

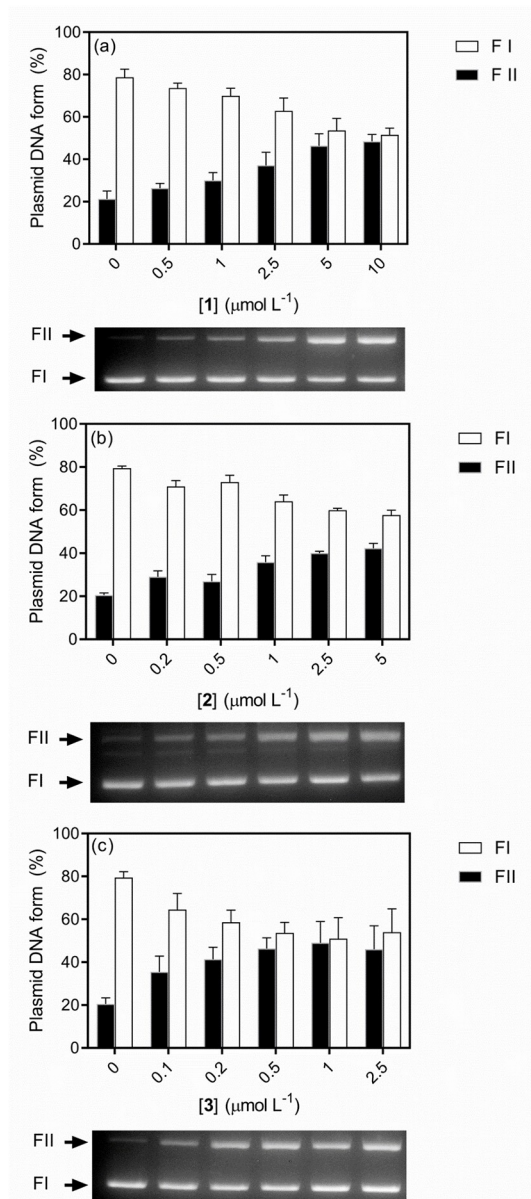


Figure 7. Cleavage of supercoiled plasmid DNA by complexes 1 (a), 2 (b) and 3 (c) in different concentrations. Reaction conditions: [1] = 0–10 $\mu\text{mol L}^{-1}$, [2] = 0–5 $\mu\text{mol L}^{-1}$, [3] = 0–2.5 $\mu\text{mol L}^{-1}$, [DNA] = 330 ng (25 $\mu\text{mol L}^{-1}$), [Buffer] = MES (10 mmol L^{-1} , pH 6.0), $T = 50^\circ\text{C}$, $t = 4$ h.

the six-membered ring on the hard side of the complex favored both an increase in k_{cat} and a decrease in K_{M} .

In relation to other binuclear copper(II) complexes described in the literature,^[5f,28] complexes 1, 2 and 3 present a notable increase in the k_{cat} value, while the K_{M} value remains of the same order of magnitude. Thus, the affinity of the complexes for DNA is similar, but the turnover number is higher for complexes 1, 2 and 3 and therefore they are more efficient catalytic models. Also, all three complexes can accelerate DNA breakdown by a factor of more than a million.

The reactivity characteristics of the complexes described in this work situate them between one of the most efficient and

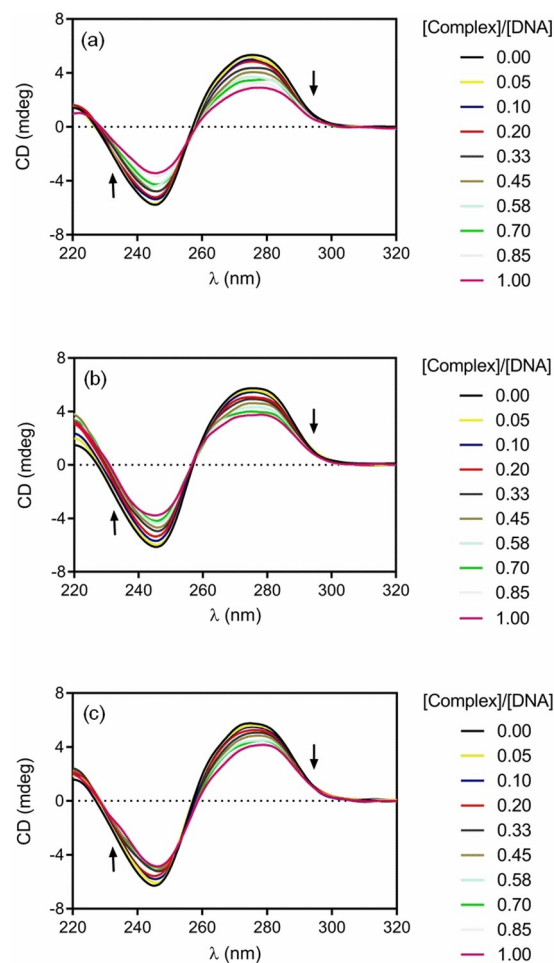


Figure 8. DNA circular dichroism spectra obtained in the presence of increasing concentrations of the complexes in acetonitrile: (a) 1, (b) 2 and (c) 3. Reaction conditions: [CT-DNA] = 200 $\mu\text{mol L}^{-1}$, [Buffer] = MES (10 mmol L^{-1} , pH 6.0), [Complex] = 0–200 $\mu\text{mol L}^{-1}$, [solvent]/[DNA] = 0–1, $T = 37^\circ\text{C}$.

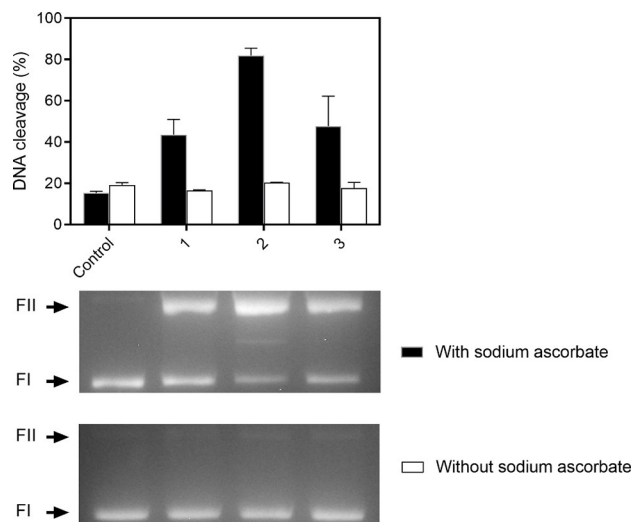


Figure 9. Cleavage of supercoiled plasmid DNA by the complexes with and without sodium ascorbate. Reaction conditions: [DNA] = 330 ng (25 $\mu\text{mol L}^{-1}$), [Buffer] = MES (10 mmol L^{-1} , pH 6.0), [Complex] = 10 $\mu\text{mol L}^{-1}$, [Sodium ascorbate] = 100 $\mu\text{mol L}^{-1}$, $T = 37^\circ\text{C}$, $t = 1$ h.

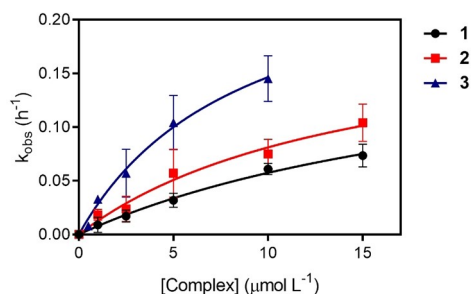


Figure 10. Plot of k_{obs} versus concentration of complexes 1, 2 and 3. Reaction conditions: [DNA] = 330 ng ($25 \mu\text{mol L}^{-1}$), [Buffer] = MES (10 mmol L^{-1} , pH 6.0), [1] = [2] = $1\text{--}15 \mu\text{mol L}^{-1}$, [3] = $0.05\text{--}10 \mu\text{mol L}^{-1}$, $T = 50^\circ\text{C}$, $t = 0\text{--}4 \text{ h}$ sheltered from light.

with the added versatility to be modulated by redox conditions of the reaction medium, a condition that is not always present for these type of metal complexes.^[10a] When a reductant was added the increase in DNA cleavage may attain a 10 times better performance which is quite interesting when different intracellular environments are targeted by the complexes.

In silico molecular docking analysis

In order to visualize the plausible interactions between the complexes studied and DNA, molecular docking calculations were performed for complexes 1–3 with a synthetic-DNA duplex with the dodecamer d(GCAAATTTGC)₂ (PDB ID: 1RVH)^[30] and the most favorable docked poses are given in Figure 11.

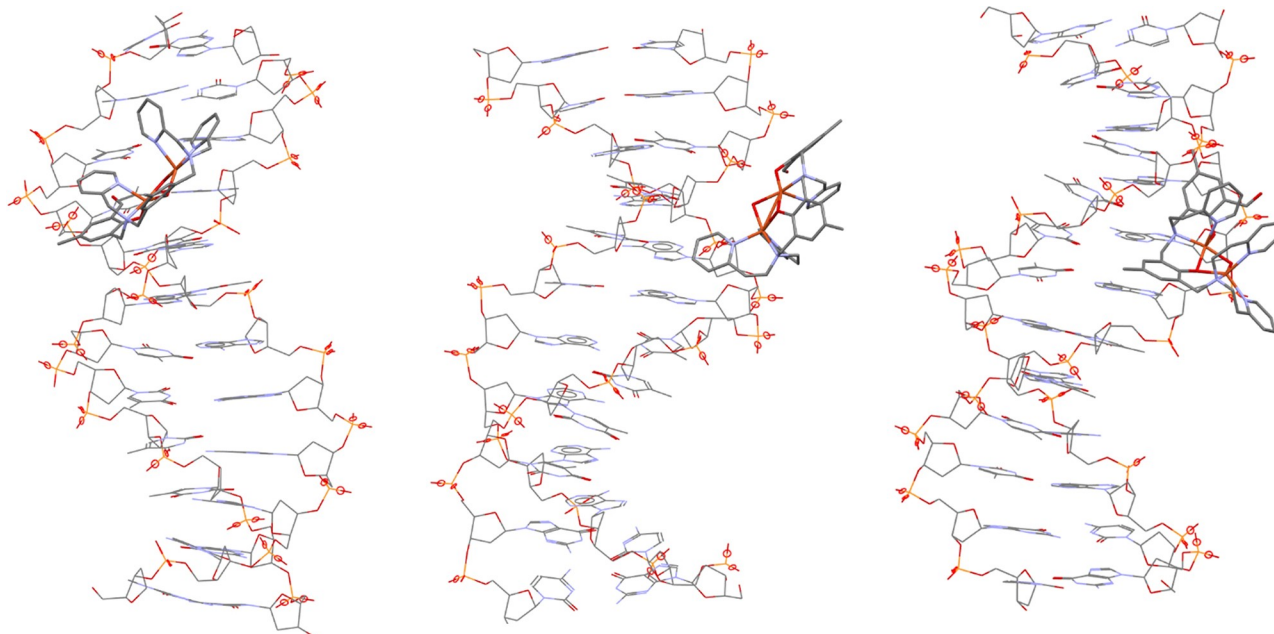


Figure 11. Molecular docking model for complexes 1 (left), 2 (middle), and 3 (right) with DNA dodecamer d(GCAAATTTGC)₂ (PDB ID: 1RVH). Calculations were done using the Patchdock[®] server.

All complexes (1–3) were best anchored in the minor groove of the DNA, driven by hydrogen bonding in hydrophobic and electrostatic interactions, where the bridging phenolate moieties are directed to the outside region of the groove. Clearly, the number of methylene groups present in the pyridine pendant arms influences the docking process. Considering Figure 11 (left), complex 1 is well fitted inside the minor groove of the DNA-dodecamer. As the number of methylene groups in complexes 2 and 3 increases (Figure 11, middle and right) the docking process seemed to be less effective. This could be related to the different conformational possibilities for 2 and 3 compared with 1.

Furthermore, no signs of intercalation processes between the nitrogen bases of the DNA and the pyridine rings from the metal complexes were observed. This finding corroborates the CD measurements discussed above as well as the results of the cleavage tests with variable ionic strength, which confirm the presence of the electrostatic interaction mode in the DNA-complex adducts.

The greater conformational variability for complexes 2 and 3 was also reflected in the fact that, besides the interaction with the minor groove, both complexes also presented docking solutions considering the major groove of DNA (Figure S42). These results are in full agreement with the DNA cleavage tests carried out for complexes 1–3 using minor and major groove ligands, such as netropsin and methyl green, respectively, where the non-specificity of the metal complexes was probed.

Conclusions

N,O-donor ligands containing different numbers of aliphatic carbon atoms, as well as their respective, as yet unpublished, dinuclear copper(II) complexes, were synthesized. Altering the number of chelate ring members in the complexes modified the acidity of the water molecules coordinated to the metal centers, as well as the electronic and $E_{1/2}$ properties of the complexes.

For these complexes, **1** is formed of only five-membered chelate rings, while in complexes **2** and **3** these rings are increased to form six-membered chelate rings, raising the flexibility of the ligand and consequently enabling it to accommodate the substrate better. DFT analysis from the optimized ground state suggested that increasing the size of the chelate ring distorts the geometry environment around both Cu atoms from an intermediate geometry between square pyramidal and trigonal-bipyramidal geometry in **1** to a mostly distorted trigonal-bipyramidal geometry in **2** and **3**.

The complexes synthesized act as biomimetic models for catechol oxidase, but the catalysis mechanism differs from that proposed for the enzyme, generating hydrogen peroxide instead of water during the cycle. In the oxidation of 3,5-DTBC, complex **2** had the highest catalytic activity and efficiency of the series. Regarding the cleavage of plasmid DNA, complex **3** was the most efficient. The change from five to six members in the chelate rings on the soft side of the complex contributed positively in both cases. The modification on the hard side, creating one more six-membered chelate ring, induced a decrease in K_M in both cases, but the change in k_{cat} varied for the reactions.

The interaction between the complexes and DNA occurred through electrostatic attraction and binding to the major and minor grooves, changing the stacking of the nitrogenous bases and the B form helicity. DNA cleavage occurred through an oxidative mechanism even in the absence of co-reagents, and all complexes catalyzed DNA cleavage (accelerated by a factor of over a million). The activity of the complexes can be modulated by the addition of a reducing agent, with a 2 to 9-fold increase in the cleavage at a lower temperature and in a shorter reaction time.

Experimental Section

Materials. The reagents and solvents used were obtained from commercial sources and employed without prior purification. The complex and substrate solutions were prepared with spectroscopic solvents and the gases used in the tests were analytical grade. The reagents used in the DNA cleavage were molecular biology grade and all solutions were prepared with Milli-Q ultrapure water. These solutions were previously sterilized using 0.22 μm Milllex membrane filters (Millipore, USA) to avoid bacterial contamination.

Physical measurements. Infrared spectra were obtained on a PerkinElmer Fourier transform infrared - attenuated total reflection (FTIR-ATR) Spectrum 100 spectrophotometer, using a crystal of ZnSe (45°), and a triglycine sulfate detector. The samples were analyzed directly with the crystal by ATR, averaging 10 scans in the range of 4000–550 cm^{-1} at a resolution of 4 cm^{-1} . The elemental

analysis of all complexes was carried out with a C, H, N and S PerkinElmer 2400 analyzer at 25 °C. The mass spectra were obtained using mass spectrometry with electrospray ionization (ESI-MS) on an Amazon-ion trap mass spectrometer. The ESI-MS analysis was carried out with acetonitrile solutions of the ligands and methanolic solutions of the complexes at a concentration of 500 ppb at 180 $\mu\text{L min}^{-1}$. The capillary temperature was maintained at 180 to 200 °C and the voltage at –3500 to –4500 V. $^1\text{H NMR}$ spectra of the ligands were obtained on a Bruker Avance 200 MHz spectrometer at room temperature. The samples were dissolved in deuterated chloroform and the internal reference used was tetramethylsilane ($\delta = 0.00$ ppm). For the copper, atomic absorption spectrometry was carried out with an Analytik Jena ContraAA 700 continuous-source high-resolution atomic absorption spectrometer, coupled with graphite furnace and flame atomizers. Complex solutions were prepared in milli-Q water containing 1% HCl. The selected wavelength was 324 nm. A mixture of air (oxidant) and acetylene (fuel) was used with a continuous flow of 60 L h^{-1} . The burner height was fixed at 16 mm.

The redox behavior of the complexes was investigated by square-wave voltammetry in a Basi potentiostat/galvanostat (model Epsilon). The concentration of the complexes was 1.0×10^{-3} mol L^{-1} in methanol at specific pH values under an argon atmosphere and with 0.1 mol L^{-1} NaClO_4 as the supporting electrolyte. The electrolytic cell contained three electrodes: glassy carbon (working); platinum wire (counter); and Ag/Ag^+ (reference). The ferrocenium/ferrocene (Fc^+/Fc) couple ($E_{1/2} = 400$ mV vs NHE^[31]) was used as the internal standard. The electronic absorption spectra were obtained on a Varian Cary 50 Bio spectrophotometer in the range of 300–850 nm with solutions of CH_3OH .

The pKa values were determined by spectrophotometric titration, with experiments performed in $\text{CH}_3\text{OH}/\text{H}_2\text{O}$ (50:50, v/v%) in a thermostatic bath (Visomes Plus) stabilized at 25.0 ± 0.5 °C. The ionic strength of the medium was adjusted with the addition of KCl (0.1 mol L^{-1}). At each pH variation of 0.1, an aliquot was removed and analyzed on a Perkin-Elmer Lambda 750 spectrophotometer. The data were fitted to sigmoidal curves and the pKa values were obtained from the inflection point. Species distribution as a function of pH was obtained for each complex using the SPECIES program.

Catecholase activity. The catalytic activity of the complexes was investigated through the oxidation of the 3,5-di-*tert*-butylcatechol (3,5-DTBC) substrate to form 3,5-di-*tert*-butylquinone (3,5-DTBQ). This reaction was monitored using a Varian Cary 50 BIO UV-Vis spectrometer coupled to a thermostatic bath. The kinetic medium used in all reactions was a $\text{CH}_3\text{OH}/\text{H}_2\text{O}$ solution (32:1, v/v), in which the absorption coefficient of the quinone formed is 1645 $\text{L mol}^{-1} \text{cm}^{-1}$ at 400 nm.^[59] The effects of pH (buffer solutions of 2-(*N*-morpholino)ethanesulfonic acid-MES- and Tris (hydroxymethyl)aminomethane-TRIS – pH 6.0 to 9.0), substrate concentration (0.5 to 14.5 mmol L^{-1}) and oxygen (inert atmosphere) on the 3,5-DTBC oxidation were evaluated. The parameters used are described in Table 5.

In a typical kinetic procedure, aqueous buffer solution, methanolic solution of a complex (**1**, **2** or **3**) and methanol saturated with oxygen or argon were added to glass cuvettes with 1-cm path length. After 10 min of incubation, the reaction was initiated with the addition of a methanolic solution of the 3,5-DTBC substrate and maintained at 25 °C. For the oxidation of 3,5-DTBC in an inert atmosphere, the solutions used were prepared in argon-saturated spectroscopic-grade methanol. At the end of the additions, carried out in argon (constant flow), the cuvette was closed. After 20 min of reaction, oxygen in the cuvette was purged to reveal possible spectral changes. Corrections for the spontaneous oxidation of 3,5-

Table 5. Experimental conditions applied in catecholase activity tests at 25 °C.

Effect	pH ^[a]	[3,5-DTBC] [mmol L ⁻¹]	Saturation gas	[Complex] [μmol L ⁻¹] ^[b]		
				1	2	3
pH	6.0–9.0	5.0	O ₂	59	16	27
Substrate	9.0	0.5–14.5	O ₂	60	60	60
Inert atmosphere	9.0	0.2	Ar	50	50	50
Presence of H ₂ O ₂	9.0	60.0	O ₂	50	50	50

[a] For all experiments, [buffer] = 30.3 mmol L⁻¹. [b] Each test was conducted with only one complex: 1, 2, or 3.

DTBC were performed by monitoring reactions under the same conditions, but in the absence of a complex.

The presence of H₂O₂ in the oxidation reactions was investigated through a modified iodometry method.^[59] The reaction mixture was prepared similarly to that mentioned for the kinetic procedure, but with different experimental parameters (Table 5). After one hour, an equal volume of water was added and the 3,5-DTBQ was extracted with dichloromethane. The aqueous layer was acidified with sulfuric acid (pH ≈ 2). A 2 mL aliquot was collected, and 1 mL of aqueous potassium iodide solution (0.3 mol L⁻¹) was added to this sample. If hydrogen peroxide is present in the aqueous phase, the following reaction occurs: H₂O₂ + 2I⁻ + 2H⁺ → 2H₂O + I₂. Iodide excess in the solution generates the triiodide ion (I_{2(aq)} + I⁻ → I₃⁻), which can be monitored by UV/Vis spectroscopy due to the appearance of an intense band at 353 nm (ε = 26000 L mol⁻¹ cm⁻¹).^[32]

DNA cleavage activity. The DNA cleavage experiments were performed as described by Ausubel et al.^[33] Plasmid DNA, used as the substrate, was extracted from plasmid pBSK-II (2961 bp, Stratagene). The plasmid was amplified by transformation into competent cells of the bacterium DH5-α *Escherichia coli* according to a procedure previously described^[34] and purified using the manufacturer's protocol (Qiagen Plasmid Maxi Kit protocol). The DNA substrate was quantified via UV-Vis spectroscopy at 260 nm (ε = 13200 L mol⁻¹ cm⁻¹) and its integrity was verified via gel electrophoresis.^[35]

In a typical DNA cleavage reaction, 2 μL of pBSK-II DNA (330 ng; 25 μmol L⁻¹), 2 μL of biological buffer, 5 μL of complex solution and 11 μL of autoclaved Milli-Q water were added. After 4 h at 50 °C, the reaction was terminated by the addition of 5 μL of running buffer (0.25 mol L⁻¹ EDTA at pH 8.0, 50% glycerol and 0.01% bromophenol blue). The samples were applied to an agarose gel (1%) containing ethidium bromide (0.3 μg mL⁻¹) and electrophoresed for 100 min at 90 V in 0.5 × TBE buffer (44.5 mmol L⁻¹ TRIS, 44.5 mmol L⁻¹ boric acid, 1 mmol L⁻¹ EDTA at pH 8.0). After the runs, the gels were visualized and recorded using the DigiDoc-It photo-documentation system (UVP, USA). The fractions of each plasmid DNA shape were quantified by densitometry using the KODAK Molecular Imaging Software 5.0 (Carestream Health, USA). Since the ability of ethidium bromide to intercalate into supercoiled DNA (form I) is less efficient than into other forms, that is, open circular (form II) and linear (form III), the values found for form I were multiplied by a correction factor of 1.47 and the values obtained for the other forms were corrected by proportionality.^[36] The amount of cleaved DNA (%) was considered to be the sum of DNA fractions in form II and form III.

The effect of pH on DNA cleavage reactions was evaluated for each complex (10 μmol L⁻¹) using different buffers: MES (pH 6.0), 4-(2-hydroxyethyl)-1-piperazineethanesulfonic acid – HEPES (pH 7.0 and 8.0), 2-(cyclohexylamino)ethanesulfonic acid – CHES (pH 9.0) and 3-(cyclohexylamino)-1-propanesulfonic acid – CAPS (pH 10.0). Thus,

to verify the mechanism of DNA cleavage by the complexes, external agents were added to the reaction mixtures before each complex. The ionic strength of the reaction was modified by replacing water with NaCl or LiClO₄ solutions at 15, 30, 75 and 125 mmol L⁻¹. The reactions were also performed with groove binders by replacing 4 μL of water with groove binder stock solutions (50 μmol L⁻¹). The compounds used to bind to the major and minor groove of DNA were methyl green (MG) and netropsin (Net), respectively.^[37] In this case, binders were incubated with DNA at pH 6.0 for 30 min in the absence of light. In addition, the effect of reactive oxygen species (ROS) was evaluated by replacing 4 μL of water with an ROS sequesterant solution: ethanol (0.4 mmol L⁻¹), potassium iodide (0.5 mmol L⁻¹) or sodium azide (0.5 mmol L⁻¹). Modulation of plasmid DNA cleavage was performed by adding 10 μL of sodium ascorbate stock solution (100 μmol L⁻¹) instead of water. Reactions occurred in the presence of 10 μmol L⁻¹ of the complexes for 1 h at 37 °C or 4 h at 50 °C.

Anaerobic tests were conducted and, to maintain an oxygen-free environment, all experimental procedures were performed in a glove bag. For these assays, two controls were performed: one with CH₃CN as the negative cleavage control and one containing 2 μL Fe-EDTA (1 mmol L⁻¹ / 2 mmol L⁻¹) and 2 μL DTT (10 mmol L⁻¹) as a positive control to replace the complex solution.^[38]

The DNA cleavage kinetics was investigated with a mixture containing 14 μL pBSK-II DNA (25 μmol L⁻¹), 14 μL MES buffer (10 mmol L⁻¹), 77 μL water and 35 μL complex solution in different concentrations ([1] = [2] = 1.0, 2.5, 5.0, 10.0 and 15.0 μmol L⁻¹; [3] = 0.05, 1.0, 2.5, 5.0 and 10.0 μmol L⁻¹). This reaction system was kept at 50 °C and aliquots were taken at regular times. After each aliquot had been removed, 5 μL of running buffer was added to it to complete the cleavage reaction. The samples were then submitted to agarose gel electrophoresis. In all experiments, reactions under the same conditions without the presence of complexes were performed as a control to monitor the spontaneous degradation of plasmid DNA.

Circular dichroism spectra were obtained with the JASCO J-815 CD spectropolarimeter (Jasco, USA). The experiments were performed with a 2 mm-optical path quartz cuvette containing 40 μL MES buffer (10 mmol L⁻¹), 80 μL CT-DNA stock solution (200 μmol L⁻¹) and 280 μL water. CT-DNA was titrated with 200 μM of solutions with [complex]/[DNA] ratios from 0.05 to 1. The CD spectra were obtained in triplicate, with each scan resulting from the accumulation of three spectra. Spectra were also obtained in the absence of CT-DNA and complex (blank). Spectra of the complexes in the absence of DNA were also obtained and showed no significant signals.

Theoretical predictions. Optimization of the geometry of complexes 1, 2 and 3 was carried out in vacuum with the Orca 4.2.1 software package^[39] at the DFT level using the BP86 functional.^[40] The basis set chosen was Def2-TZVP for the copper atom and Def2-SVP for the other atoms.^[41] Our calculations also included Grimme's dispersion correction (D3) with Becke-Johnson damping (BJ)^[42] The vibrational frequencies for complexes 1, 2 and 3 showed only one small imaginary frequency for complex 3 due to rotation of the aromatic rings. The 3,5-DTBC conjugates were also optimized and the vibrational frequencies showed one small negative frequency due to rotation of the aromatic rings. In order to simulate the absorption spectra, time-dependent density functional theory under the Tamm-Dancoff approximation (TD-DFT/TDA)^[43] was employed to obtain the first 30 excitations, using the same calculation protocol, differing only at the functional, which in this case was PBE0^[44] and the basis set for coordinated atoms chosen was the same used for the copper atom (Def2-TZVP). To include the solvent effects in the excited state energies, the conductor-like

polarizable continuum model (CPCM)^[45] was used, with methanol as the solvent. The 3D representations of the complexes were obtained using the Chemcraft program.^[46]

In silico analysis via Patchdock®. *In silico* analysis (binding mode) for complexes 1–3 with double-stranded DNA was carried out using the online Patchdock server.^[46] The B-DNA dodecamer was retrieved from the Protein Data Bank (PDB ID: 1RVH).^[30] All possible poses were considered as starting points and the docking analysis were performed. The default parameters were used for the docking calculation. Visualization of the docked systems was further analyzed with the Mercury software.^[48]

Synthesis of copper(II) complexes. The ligand H₂L₁ (Figure 1 and Figure S1) was synthesized according to a previously reported protocol.^[12a] The ligands H₂L₂ and H₂L₃ (Figure 1 and Figures S2 and S3, respectively) were synthesized according to the procedure described in the Supporting Information.^[12b]

The complexes were synthesized by adding 10 mL of a methanolic solution containing 1.0 mmol of copper(II) perchlorate hexahydrate (0.37 g; 370.54 g mol⁻¹) to another methanolic solution (40 mL) containing 0.5 mmol of ligand (H₂L₁ – 0.29 g, 587.29 g mol⁻¹; H₂L₂ – 0.31 g, 615.32 g mol⁻¹; and H₂L₃ – 0.31 g, 629.34 g mol⁻¹), under stirring at 40 °C. The mixture was stirred for 10 min and 0.5 mL of a NaOH solution (1 mol L⁻¹) was then added. The green solution was filtered and left to stand at room temperature for slow evaporation of the remaining solvent. The crude product was obtained as a powder, washed several times with water, washed with isopropanol and diethyl ether and used without further purification.

[Cu^{II}(μ-OH)Cu^{II}(L₁)](ClO₄)₂·NaClO₄ Complex (1). Yield: 75%. IR – KBr pellets (cm⁻¹): ν(O–H) 3534, ν(C–H_{Arr}, C–H_{aliph} and C–H_{aldehyde}) 3080–2864, ν(C=O_{ald}) 1648, ν(C=C and C=N) 1609–1444, δ(O–H) 1382, ν(Cl–O) 1070, δ(C–H_{Ar}) 769, δ(C=C_{Ar}) 616. Atomic absorption (mg kg⁻¹) – Cu: 3.057 ± 0.017. Elemental analysis calcd (%): C 41.60, H 3.87, N 6.56; found: C 41.45, H 3.95, N 6.37.

[Cu^{II}(μ-OCH₃)Cu^{II}(L₂)](ClO₄)₂ Complex (2). Yield: 72%. IR – KBr pellets (cm⁻¹): ν(O–H) 3534, ν(C–H_{Arr}, C–H_{aliph} and C–H_{aldehyde}) 3080–2864, ν(C=O_{ald}) 1648, ν(C=C and C=N) 1609–1444, δ(O–H) 1382, ν(Cl–O) 1070, δ(C–H_{Ar}) 769, δ(C=C_{Ar}) 616. Atomic absorption (mg kg⁻¹) – Cu: 3.294 ± 0.027. Elemental analysis calcd (%): C 47.65, H 4.31, N 7.31; found: C 47.39, H 4.12, N 7.64.

[Cu^{II}(μ-OCH₃)Cu^{II}(L₃)](ClO₄)₂·NaClO₄·CH₃OH Complex (3). Yield: 72%. IR – KBr pellets (cm⁻¹): ν(O–H) 3534, ν(C–H_{Arr}, C–H_{aliph} and C–H_{aldehyde}) 3080–2864, ν(C=O_{ald}) 1648, ν(C=C and C=N) 1609–1444, δ(O–H) 1382, ν(Cl–O) 1070, δ(C–H_{Ar}) 769, δ(C=C_{Ar}) 616. Atomic absorption (mg kg⁻¹) – Cu: 2.616 ± 0.006. Elemental analysis calcd (%): C 43.19, H 4.33, N 6.14; found: C 43.33, H 4.41, N 5.88.

Acknowledgements

This study was financed in part by the Coordenação de Aperfeiçoamento de Pessoal de Nível Superior – Brasil (CAPES) – Finance Code 001. The authors also thank National Counsel of Technological and Scientific Development (CNPq-Brazil).

Conflict of Interest

The authors declare no conflict of interest.

Keywords: Biomimetic studies · Catecholase activity · Copper · Density functional calculations · DNA cleavage

- [1] a) C. Eicken, B. Krebs, J. C. Sacchetti, *Curr. Opin. Struct. Biol.* **1999**, *9*, 677–683; b) C. Gerdemann, C. Eicken, B. Krebs, *Acc. Chem. Res.* **2002**, *35*, 183–191.
- [2] a) H. Jiang, W. Lai, *Org. Biomol. Chem.* **2020**, *18*, 5192–5202; b) C. A. Ramsden, P. A. Riley, *Bioorg. Med. Chem.* **2014**, *22*, 2388–2395; c) B. Singh, K. Suri, K. Shevkani, A. Kaur, A. Kaur, N. Singh, in *Enzym. Food Technol.*, Springer Singapore, Singapore, **2018**, pp. 63–78.
- [3] T. Klabunde, C. Eicken, J. C. Sacchetti, B. Krebs, *Nat. Struct. Biol.* **1998**, *5*, 1084–1090.
- [4] a) S. K. Dey, A. Mukherjee, *Coord. Chem. Rev.* **2016**, *310*, 80–115; b) R. El Ati, A. Takfaoui, M. El Kodadi, R. Touzani, E. B. Yousfi, F. A. Almalki, T. Ben Hadda, *Mater. Today: Proc.* **2019**, *13*, 1229–1237; c) I. A. Koval, K. Selmececi, C. Belle, C. Philouze, E. Saint-Aman, I. Gautier-Luneau, A. M. Schuitema, M. van Vliet, P. Gamez, O. Roubeau, M. Lügen, B. Krebs, M. Lutz, A. L. Spek, J.-L. Pierre, J. Reedijk, *Chem. A Eur. J.* **2006**, *12*, 6138–6150; d) S. K. Dey, A. Mukherjee, *New J. Chem.* **2014**, *38*, 4985–4995; e) I. A. Koval, C. Belle, K. Selmececi, C. Philouze, E. Saint-Aman, A. M. Schuitema, P. Gamez, J.-L. Pierre, J. Reedijk, *J. Biol. Inorg. Chem.* **2005**, *10*, 739–750; f) K. Born, P. Comba, A. Daubinet, A. Fuchs, H. Wadehol, *J. Biol. Inorg. Chem.* **2006**, *12*, 36–48.
- [5] a) R. A. Peralta, A. J. Bortoluzzi, B. Szpoganicz, T. A. S. Brandão, E. E. Castellano, M. B. De Oliveira, P. C. Severino, H. Terenzi, A. Neves, *J. Phys. Org. Chem.* **2010**, *23*, 1000–1013; b) M. R. Mendoza-Quijano, G. Ferrer-Sueta, M. Flores-Alamo, N. Aliaga-Alcalde, V. Gómez-Vidales, V. M. Ugalde-Saldívar, L. Gasque, *Dalton Trans.* **2012**, *41*, 4985; c) S. Mukherjee, T. Weyhermüller, E. Bothe, K. Wiegardt, P. Chaudhuri, *Dalton Trans.* **2004**, 3842–3853; d) L. Paul, B. Banerjee, A. Bhaumik, M. Ali, *Microporous Mesoporous Mater.* **2017**, *249*, 78–87; e) D. Mondal, M. Chandra Majee, *Inorg. Chim. Acta* **2017**, *465*, 70–77; f) R. E. H. M. B. Osório, R. A. Peralta, A. J. Bortoluzzi, V. R. De Almeida, B. Szpoganicz, F. L. Fischer, H. Terenzi, A. S. Mangrich, K. M. Mantovani, D. E. C. Ferreira, W. R. Rocha, W. Haase, Z. Tomkowicz, A. Dos Anjos, A. Neves, *Inorg. Chem.* **2012**, *51*, 1569–1589; g) T. P. Camargo, F. F. Maia, C. Chaves, B. de Souza, A. J. Bortoluzzi, N. Castilho, T. Bortolotto, H. Terenzi, E. E. Castellano, W. Haase, Z. Tomkowicz, R. A. Peralta, A. Neves, *J. Inorg. Biochem.* **2015**, *146*, 77–88; h) A. Neves, A. J. Bortoluzzi, R. Jovito, R. A. Peralta, B. de Souza, B. Szpoganicz, A. C. Joussef, H. Terenzi, P. C. Severino, F. L. Fischer, G. Schenck, M. J. Riley, S. J. Smith, L. R. Gahan, *J. Braz. Chem. Soc.* **2010**, *21*, 1201–1212.
- [6] a) I. A. Koval, P. Gamez, C. Belle, K. Selmececi, J. Reedijk, *Chem. Soc. Rev.* **2006**, *35*, 814; b) P. E. M. Siegbahn, *J. Biol. Inorg. Chem.* **2004**, *9*, 577–590; c) S. Dutta, P. Bhunia, J. Mayans, M. G. B. Drew, A. Ghosh, *Dalton Trans.* **2020**, *49*, 11268–11281.
- [7] A. Terán, A. Jaafar, A. E. Sánchez-Peláez, M. C. Torralba, Á. Gutiérrez, *J. Biol. Inorg. Chem.* **2020**, *25*, 671–683.
- [8] a) M. Hasanazadeh Esfahani, M. Behzad, *J. Coord. Chem.* **2020**, 1–10; b) R. M. Gandra, P. Mc Carron, M. F. Fernandes, L. S. Ramos, T. P. Mello, A. C. Aor, M. H. Branquinho, M. McCann, M. Devereux, A. L. S. Santos, *Front. Microbiol.* **2017**, *8*, 1257.
- [9] a) Z. Rasic-Milutinovic, D. Jovanovic, G. Bogdanovic, J. Trifunovic, J. Mutic, *Exp. Clin. Endocrinol. Diabetes* **2016**, *125*, 79–85; b) C. M. Ackerman, C. J. Chang, *J. Biol. Chem.* **2018**, *293*, 4628–4635; c) L. Fouani, S. V. Menezes, M. Paulson, D. R. Richardson, Z. Kovacevic, *Pharmacol. Res.* **2017**, *115*, 275–287; d) M. H. Raza, S. Siraj, A. Arshad, U. Waheed, F. Aldakheel, S. Alduraywish, M. Arshad, *J. Cancer Res. Clin. Oncol.* **2017**, *143*, 1789–1809; e) M. Navarro, E. J. Cisneros-Fajardo, A. Sierralta, M. Fernández-Mestre, P. Silva, D. Arrieche, E. Marchán, *J. Biol. Inorg. Chem.* **2003**, *8*, 401–408; f) G.-Y. Li, K.-J. Du, J.-Q. Wang, J.-W. Liang, J.-F. Kou, X.-J. Hou, L.-N. Ji, H. Chao, *J. Inorg. Biochem.* **2013**, *119*, 43–53.
- [10] a) A. Erxleben, *Coord. Chem. Rev.* **2018**, *360*, 92–121; b) Z. Molphy, A. Priscarú, C. Slator, N. Barron, M. McCann, J. Collieran, D. Chandran, N. Gathergood, A. Kellett, *Inorg. Chem.* **2014**, *53*, 5392–5404; c) T. J. P. McGivern, S. Afsharpour, C. J. Marmion, *Inorg. Chim. Acta* **2018**, *472*, 12–39; d) N. Shahabadi, M. Hakimi, T. Morovati, M. Falsafi, S. M. Fili, *J. Photochem. Photobiol. B* **2017**, *167*, 7–14; e) D. Anu, P. Naveen, B. Vijaya Pandiyan, C. S. Frampton, M. V. Kaveri, *Polyhedron* **2019**, *167*, 137–150.
- [11] a) S. Anbu, M. Kandaswamy, P. Suthakaran, V. Murugan, B. Varghese, *J. Inorg. Biochem.* **2009**, *103*, 401–410; b) F. Xue, C.-Z. Xie, Y.-W. Zhang, Z. Qiao, X. Qiao, J.-Y. Xu, S.-P. Yan, *J. Inorg. Biochem.* **2012**, *115*, 78–86;

- c) R. A. Peralta, A. Neves, A. J. Bortoluzzi, A. dos Anjos, F. R. Xavier, B. Szpoganicz, H. Terenzi, M. C. B. de Oliveira, E. Castellano, G. R. Friedermann, A. S. Mangrich, M. A. Novak, *J. Inorg. Biochem.* **2006**, *100*, 992–1004.
- [12] a) C. Piovezan, R. Jovito, A. J. Bortoluzzi, H. Terenzi, F. L. Fischer, P. C. Severino, C. T. Pich, G. G. Azzolini, R. A. Peralta, L. M. Rossi, A. Neves, *Inorg. Chem.* **2010**, *49*, 2580–2582; b) C. Pereira, G. Farias, F. G. Maranhã, N. Castilho, G. Schenk, B. de Souza, H. Terenzi, A. Neves, R. A. Peralta, *J. Biol. Inorg. Chem.* **2019**, *24*, 675–691.
- [13] K. Nakamoto, *Infrared and raman spectra of inorganic and coordination compounds in Handbook of Vibrational Spectroscopy*, John Wiley & Sons, New York, **2006**, pp. 1872–1892.
- [14] M. S. Ahmad, M. Khalid, M. S. Khan, M. Shahid, M. Ahmad, Monika, A. Ansari, M. Ashafaq, *New J. Chem.* **2020**, *44*, 7998–8009.
- [15] H. Ünver, Z. Hayvali, *Spectrochim. Acta Part A* **2010**, *75*, 782–788.
- [16] a) T. P. Camargo, R. A. Peralta, R. Moreira, E. E. Castellano, A. J. Bortoluzzi, A. Neves, *Inorg. Chem. Commun.* **2013**, *37*, 34–38; b) L. R. Martins, E. T. Souza, T. L. Fernandez, B. de Souza, S. Rachinski, C. B. Pinheiro, R. B. Faria, A. Casellato, S. P. Machado, A. S. Mangrich, M. Scarpellini, *J. Braz. Chem. Soc.* **2010**, *21*, 1218–1229; c) M. Schatz, M. Becker, F. Thaler, F. Hampel, S. Schindler, R. R. Jacobson, Z. Tyeklár, N. N. Murthy, P. Ghosh, Q. Chen, J. Zubieta, K. D. Karlin, *Inorg. Chem.* **2001**, *40*, 2312–2322.
- [17] S. Ghosh, J. Cirera, M. A. Vance, T. Ono, K. Fujisawa, E. I. Solomon, *J. Am. Chem. Soc.* **2008**, *130*, 16262–16273.
- [18] E. A. Ambundo, M.-V. Deydier, A. J. Grall, N. Aguera-Vega, L. T. Dressel, T. H. Cooper, M. J. Heeg, L. A. Ochrymowycz, D. B. Rorabacher, *Inorg. Chem.* **1999**, *38*, 4233–4242.
- [19] A. Neves, L. M. Rossi, A. J. Bortoluzzi, B. Szpoganicz, C. Wieszicki, E. Schwingel, W. Haase, S. Ostrovsky, *Inorg. Chem.* **2002**, *41*, 1788–1794.
- [20] a) S. Torelli, C. Belle, S. Hamman, J. L. Pierre, E. Saint-Aman, *Inorg. Chem.* **2002**, *41*, 3983–3989; b) C. Fernandes, A. Neves, A. J. Bortoluzzi, A. S. Mangrich, E. Rentschler, B. Szpoganicz, E. Schwingel, *Inorg. Chim. Acta* **2001**, *320*, 12–21.
- [21] Z. Yu, J. Cowan, *Curr. Opin. Chem. Biol.* **2018**, *43*, 37–42.
- [22] J.-A. Ma, *Chem. Soc. Rev.* **2006**, *35*, 630–636.
- [23] a) S. R. U. Joy, E. Trufan, M. D. Smith, C. Puscas, R. L. Silaghi-Dumitrescu, R. F. Semeniuc, *Inorg. Chim. Acta* **2019**, *485*, 190–199; b) S. Caglar, E. Adiguzel, B. Sariboga, E. Temel, O. Buyukgungor, *J. Coord. Chem.* **2014**, *67*, 670–683; c) B. Zheng, H. Liu, J. Feng, J. Zhang, *Appl. Organomet. Chem.* **2014**, *28*, 372–378; d) J. Adhikary, P. Chakraborty, S. Das, T. Chattopadhyay, A. Bauzá, S. K. Chattopadhyay, B. Ghosh, F. A. Mautner, A. Frontera, D. Das, *Inorg. Chem.* **2013**, *52*, 13442–13452.
- [24] G. A. D. S. Silva, A. L. Amorim, B. De Souza, P. Gabriel, H. Terenzi, E. Nordlander, A. Neves, R. A. Peralta, *Dalton Trans.* **2017**, *46*, 11380–11394.
- [25] K. Jumbri, H. Ahmad, E. Abdulmalek, M. B. Abdul Rahman, *J. Mol. Liq.* **2016**, *223*, 1197–1203.
- [26] a) S. Parodi, F. Kendall, C. Nicolini, *Nucleic Acids Res.* **1975**, *2*, 477–486; b) B. Nordén, F. Tjerneld, *Biopolymers* **1982**, *21*, 1713–1734; c) F. Tavakolyanpour, S. Waqif Husain, M. H. Rastegar, M. Saber Tehrani, P. Abroomand Azar, A. A. Momtazi Borojeni, S. Alireza Esmaili, *J. Iran. Chem. Soc.* **2016**, *13*, 2121–2133.
- [27] C. Santini, M. Pellei, V. Gandin, M. Porchia, F. Tisato, C. Marzano, *Chem. Rev.* **2014**, *114*, 815–862.
- [28] M. P. Silva, C. Saibert, T. Bortolotto, A. J. Bortoluzzi, G. Schenk, R. A. Peralta, H. Terenzi, A. Neves, *J. Inorg. Biochem.* **2020**, *213*, 111249.
- [29] M. E. Allentoft, M. Collins, D. Harker, J. Haile, C. L. Oskam, M. L. Hale, P. F. Campos, J. A. Samaniego, M. T. P. Gilbert, E. Willerslev, G. Zhang, R. P. Scofield, R. N. Holdaway, M. Bunce, *Proc. R. Soc. B Biol. Sci.* **2012**, *279*, 4724–4733.
- [30] R. Stefl, H. Wu, S. Ravindranathan, V. Sklenar, J. Feigon, *Proc. Nat. Acad. Sci.* **2004**, *101*, 1177–1182.
- [31] R. R. Gagne, C. A. Koval, G. C. Lisensky, *Inorg. Chem.* **1980**, *19*, 2854–2855.
- [32] J. Ackermann, F. Meyer, E. Kaifer, H. Pritzkow, *Chem. A Eur. J.* **2002**, *8*, 247–258.
- [33] A. Neves, H. Terenzi, R. Horner, A. Horn Jr., B. Szpoganicz, J. Sugai, *Inorg. Chem. Commun.* **2001**, *4*, 388–391.
- [34] F. M. Ausubel, R. Brent, R. E. Kingston, D. D. Moore, J. G. Seidman, J. A. Smith, K. Struhl, *Short Protocols in Molecular Biology: A Compendium of Methods from Current Protocols in Molecular Biology*, Wiley, New York, **1999**.
- [35] L. J. Cseke, J. R. Herdy, *Methods Cell Biol.* **2012**, *112*, 1–32.
- [36] Y. Jin, M. A. Lewis, N. H. Gokhale, E. C. Long, J. A. Cowan, *J. Am. Chem. Soc.* **2007**, *129*, 8353–8361.
- [37] a) S. K. Kim, B. Nordén, *FEBS Lett.* **1993**, *315*, 61–64; b) M. W. Van Dyke, R. P. Hertzberg, P. B. Dervan, *Proc. Nat. Acad. Sci.* **1982**, *79*, 5470–5474.
- [38] S. S. Massoud, R. S. Perkins, F. R. Louka, W. Xu, A. Le Roux, Q. Dutercq, R. C. Fischer, F. A. Mautner, M. Handa, Y. Hiraoka, G. L. Kreft, T. Bortolotto, H. Terenzi, *Dalton Trans.* **2014**, *43*, 10086.
- [39] F. Neese, *WIREs Comput. Mol. Sci.* **2018**, *8*, 1327.
- [40] a) A. D. Becke, *Phys. Rev. A* **1988**, *38*, 3098–3100; b) J. P. Perdew, *Phys. Rev. B* **1986**, *33*, 8822–8824.
- [41] a) A. Schäfer, H. Horn, R. Ahlrichs, *J. Chem. Phys.* **1992**, *97*, 2571–2577; b) A. Schäfer, C. Huber, R. Ahlrichs, *J. Chem. Phys.* **1994**, *100*, 5829–5835; c) F. Weigend, R. Ahlrichs, *Phys. Chem. Chem. Phys.* **2005**, *7*, 3297.
- [42] a) S. Grimme, J. Antony, S. Ehrlich, H. Krieg, *J. Chem. Phys.* **2010**, *132*, 154104; b) S. Grimme, S. Ehrlich, L. Goerigk, *J. Comput. Chem.* **2011**, *32*, 1456–1465.
- [43] T. Petrenko, S. Kossmann, F. Neese, *J. Chem. Phys.* **2011**, *134*, 054116.
- [44] a) J. P. Perdew, K. Burke, M. Ernzerhof, *Phys. Rev. Lett.* **1996**, *77*, 3865–3868; b) J. P. Perdew, K. Burke, M. Ernzerhof, *Phys. Rev. Lett.* **1997**, *78*, 1396–1396.
- [45] A. V. Marenich, C. J. Cramer, D. G. Truhlar, *J. Phys. Chem. B* **2009**, *113*, 6378–6396.
- [46] “Chemcraft,” can be found under www.chemcraftprog.com, n.d.
- [47] a) D. Duhovny, R. Nussinov, H. J. Wolfson, in *Algorithms Bioinformatics. WABI 2002. Lect. Notes Comput. Sci.* (Eds.: R. Guigó, D. Gusfield), Springer, Berlin, Heidelberg, **2002**, pp. 185–200; b) D. Schneidman-Duhovny, Y. Inbar, R. Nussinov, H. J. Wolfson, *Nucleic Acids Res.* **2005**, *33*, W363–W367.
- [48] C. F. Macrae, I. J. Bruno, J. A. Chisholm, P. R. Edgington, P. McCabe, E. Pidcock, L. Rodriguez-Monge, R. Taylor, J. van de Streek, P. A. Wood, *J. Appl. Crystallogr.* **2008**, *41*, 466–470.

Manuscript received: December 28, 2020

Revised manuscript received: March 16, 2021

Accepted manuscript online: March 22, 2021